



IUTAM Symposium on Waves in Fluids: Effects of nonlinearity, Rotation, Stratification and Dissipation

## Large scale energy transfer from an internal gravity wave reflecting on a simple slope

Nicolas Grisouard<sup>a</sup>, Matthieu Leclair<sup>b</sup>, Louis Gostiaux<sup>b,c</sup>, Chantal Staquet<sup>b\*</sup>

<sup>a</sup> Courant Institute of Mathematical Sciences, 251 Mercer Street, New York, NY 10012-1185, USA

<sup>b</sup> LEGI, UJF/CNRS/G-INP, BP 53, 38041 Grenoble cdx 9, France

<sup>c</sup> LMFA UMR 5509, CNRS, Ecole Centrale de Lyon - Universit de Lyon, Ecully, France

---

### Abstract

Several processes lead to mixing and transport in the ocean, among those being the interaction of the internal gravity wave field with bottom topography. The latter process is considered in the present work, through joint laboratory experiments and numerical simulations. The basic configuration is a plane wave of finite extent reflecting onto a sloping bottom in a uniformly stratified fluid. As expected, the interaction between the incident and reflected waves produces harmonic waves, but an irreversible wave-induced mean flow grows in the interacting region between those waves, whose amplitude may be larger than that of the incident wave. This mean flow appears to be controlled by nonlinear and dissipative effects associated with the reflected wave component. Unlike in the atmosphere, the role of this wave-induced mean flow has been completely overlooked in the ocean.

© 2012 Published by Elsevier Ltd. Selection and/or peer-review under responsibility of the Institution of the Russian Academy of Sciences A. Ishlinsky, Institute for Problems in Mechanics of the RAS.

*Keywords:* Physical Oceanography; Internal gravity waves; Solitary waves; Wave-induced mean flow; Numerical experiments; Laboratory experiments

---

### 1. Introduction

The main sources of energy for internal gravity waves in the ocean are the tide and the wind [1]. Tide flowing over the bottom topography of the ocean (the bathymetry) generates internal gravity waves referred to as the internal tide, with frequency equal to that of the tide. The wind creates internal gravity waves in the upper layer of the ocean with frequency close to the inertial frequency. Quite remarkably, these waves are able to propagate toward the bottom of the ocean ([2]); the associated process is subtle, resulting from the interaction of near-inertial waves with meso-scale turbulence in the upper layer [3]. Another process, indirectly due to the wind, currently forms a new field research. It is linked with the Antarctic Circumpolar Current in the Southern Ocean which is locally barotropic and can therefore interact with the bathymetry. Like the wind blowing over topography in the atmosphere, lee waves are very likely

---

\* Chantal Staquet. Tel.: +33-476 825 024 ; fax: +33-476-825-271 .  
E-mail address: [Chantal.Staquet@legi.grenoble-inp.fr](mailto:Chantal.Staquet@legi.grenoble-inp.fr)

generated by the Antarctic Circumpolar Current [4] whose breaking may account for intense mixing measured in the deep ocean in several regions of the Southern Ocean [5]. In the present paper we focus on the internal tide.

The interest of the oceanic community in internal gravity waves lies in their capacity to fluid mixing, especially in the deep ocean where motions are generally dominated by these waves. Mixing results from energy transfers toward small scales through various processes such as, for the internal tide, parametric sub-harmonic instability [6]. While mixing is associated with a vertical transport of heat and mass (downward and upward, respectively), internal gravity waves can also induce horizontal mass transport [7]. It is indeed well-known that waves, whether dispersive or not (such as surface gravity waves or sound waves), induce an irreversible mean flow when propagating in a dissipative medium [8]. Mixing and wave-induced mean flow may be considered as processes by which the wave-induced energy is transferred toward small and large scales respectively. While mixing has been and is still intensively studied, very little work has been performed on wave-induced mean flows in the ocean and their impact on ocean dynamics [9]. Mean flow changes by momentum deposition of the internal tide are addressed in the present paper, through the nonlinear reflection of a plane wave of finite extent onto a simple slope in a stably-stratified medium of constant Brunt-Väisälä frequency  $N$ .

In such a medium, the dispersion relation of plane internal gravity waves is

$$\omega^2 = N^2 \sin^2 \theta, \quad (1)$$

where  $\omega$  is the wave frequency (assumed to be positive) and  $\theta$ , the angle of the group velocity with the horizontal. For an object oscillating at frequency  $\omega$  in a fluid of constant  $N$  (with  $\omega < N$ ), this relation implies that the propagation of energy is anisotropic, occurring only in directions making an angle  $\theta = \arcsin(\omega/N)$  with the horizontal [10, 11] and referred to as beams.

The reflection of an incident wave onto a slope leads to a reflected wave with the same frequency  $\omega$ . The conservation of wave frequency upon reflection implies, from the anisotropic dispersion relation (1), that the angle of the group velocity  $\theta$  is also conserved upon reflection. As shown by [12], the wave may be focused upon reflection, which results in the increase of its amplitude and wavenumber by a factor  $\gamma = \sin(\theta + \alpha) / |\sin(\theta - \alpha)|$  for a slope of constant angle  $\alpha$ . For  $\theta$  close to  $\alpha$ , focusing leads to nonlinear processes [13] and organized structures sometimes referred as bores [14]. This situation is referred to as critical incidence. Away from critical incidence conditions, opportunity for nonlinear processes and therefore transport property is usually assumed to be rather rare which motivated the search for resonant interactions by [15] further discussed below.

As is well-known, the nonlinear interaction between the incident and reflected waves generates harmonic waves of frequency  $n\omega$ , which propagate if  $n\omega < N$  owing to the dispersion relation. The area where these waves superimpose, and therefore interact, will be referred to as the interaction area hereafter. The key point of the present paper is that a strong mean flow is also generated in this interaction area, the main contribution coming from the reflected wave. By *strong*, we mean that the mean flow amplitude may be larger than the incident wave amplitude. Such a mean flow has been missed in previous studies on wave reflection due to geometrical confinement. The nonlinear interaction between an incident and a reflected wave has indeed been addressed in several papers in a two-dimensional (or a quasi-two-dimensional) configuration, thereby preventing the intrinsically three-dimensional (as discussed in the section 6.2) mean flow from occurring. The seminal theoretical paper by [15] thus investigated the conditions in a  $(\alpha, \omega)$  space for an incident plane wave and its reflected counterpart to form a resonant triad with a second harmonic wave resulting from the interaction between those waves. The occurrence of such resonant interactions on a simple slope has also been investigated numerically and experimentally, but never quantitatively reproduced so far [16, 17]. In the present study, we consider the interaction of an incident and a reflected plane wave with a finite number of wavelengths in a three-dimensional configuration to allow for all components of the flow to develop.

The outline of the paper is as follows. The next section is devoted to a brief account on wave-induced mean flows. The reflection on a simple slope has been studied using laboratory experiments and both two- and three-dimensional numerical simulations. The set-ups are presented in section 3. The overall behavior of the flow as obtained from these three approaches is described in section 4 while a detailed harmonic analysis is conducted in section 5. We focus on the wave-induced mean flow in section 6 and conclude in section 7.

## 2. A brief account on wave-induced mean flow

A fundamental property of waves is they transporting the energy and the momentum of the source which creates them, without mass transport if the waves are steady, linear and non dissipative. This is the non acceleration theorem [18]. It follows that, for a small-amplitude wave, either transient or nonlinear effects accelerate the flow, thereby modifying the ambient mean flow or inducing a mean flow if the fluid is initially at rest. In a non dissipative medium, the mean flow response to wave transience or wave nonlinearity is bounded in time and reversible, while those mean flow changes may be cumulative in time and irreversible in a dissipative medium. In the latter case, mean motions can have a major effect on the flow such as interacting with the waves themselves. The amplitude of the mean flow is proportional to the square of the wave amplitude, attesting that nonlinear interactions are a basic ingredient in mean flow generation (see [19, p. 98]). An alternate argument is that a process leading to a frequency equal to  $\omega - \omega$  is required to create the mean flow.

The occurrence of a dissipative mean flow can be easily conceived from momentum conservation : as the wave progresses forward, the wave-induced momentum flux decreases through molecular effects so that momentum is deposited by the wave as it propagates. This momentum deposition may be expressed as a force exerted on the fluid, which accelerates the fluid and produces the mean flow [20].

As usual in fluid mechanics, either an Eulerian or a Lagrangian point of view can be adopted to express the flow properties and so is also for averaging. The Eulerian mean flow is obtained by computing, at a fixed position, the average of the fluid velocity over a given time. The Lagrangian mean flow is computed from the average of the velocity following the motion of a fluid particle during the same time. As shown by [21], the Lagrangian mean flow is the sum of the Eulerian mean flow and of the Stokes drift velocity. The Lagrangian mean flow may vanish while the Eulerian mean flow does not: in this case, no mass transport occurs (an example will be provided below). A Lagrangian mean flow is therefore fundamentally associated with mass transport.

## 3. Experimental and numerical setups

### 3.1. Experimental set-up

Laboratory experiments have been performed on the Coriolis Platform in Grenoble [22]. As sketched in Figure 1, a key aspect of the experiments is the use of a wave generator designed to produce a plane wave and originally designed to facilitate comparison with theoretical predictions [23]. In front of the wave generator, a sloping boundary of inclination 10%, corresponding to an angle  $\alpha \approx 5.71^\circ$  with the horizontal, extends over 4 m in the longitudinal ( $x$ ) direction and over 4.5 m in the lateral ( $y$ ) direction. The reflection region is therefore unaffected by side effects. The tank is stably-stratified with brine and an initial constant stratification profile is imposed, with  $N = 0.41 \text{ rad} \cdot \text{s}^{-1}$ . The tank is non rotating.

Experiments have been performed using different forcing frequencies  $\omega$ , and hence, from the dispersion relation, different angles  $\theta$  of the incident wave field. In the present study, we consider the flow behavior obtained for a wave period equal to 42.16 s (so that  $\omega = 2\pi/42.16 \simeq 0.15 \text{ rad} \cdot \text{s}^{-1}$ ), corresponding to  $\theta = 18.6^\circ$ . Since the slope angle  $\alpha$  is equal to  $5.71^\circ$ , the focusing factor  $\gamma$  defined in the introduction has a value of 1.84.

The generator produces a beam with 4 wavelengths, the horizontal (along the  $x$ -direction) and vertical (along the  $z$ -direction) wavelengths being 0.42 m and 0.13 m respectively; the plane of this incident beam is normal to the sloping boundary. Velocity measurements are inferred from Particle Image Velocimetry using a vertical laser sheet located in the center of the incident beam; the vertical plane of this laser sheet is referred to as the  $(x, z)$  plane in Figure 1b and in the remainder of the paper.

### 3.2. Numerical set-up

Two- and three-dimensional numerical simulations have been carried out in order to reproduce the laboratory experiments. Two different codes have been used, the Symphonie-NH ocean model developed by F. Auclair [24] and

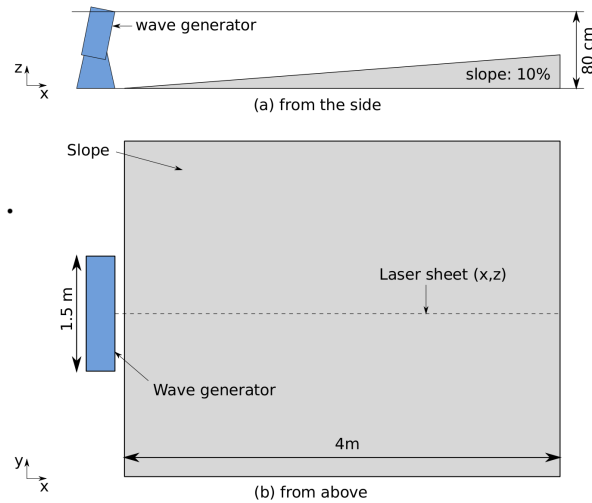


Fig. 1. Sketch of the experimental set-up viewed from the side (a) and from above (b). The dashed line in frame (b) marks the vertical laser sheet where PIV measurements are performed.

the NHOES<sup>1</sup> code written by H. Aiki [25], respectively. The major difference between these codes is the vertical coordinate, which is of the sigma-type in the former code (the sigma coordinate follows the topography, varying smoothly from the sloping boundary to the -near flat- free surface) while a cartesian coordinate is used in the NHOES code. The horizontal coordinates are of the cartesian type in both codes.

These codes solve the non hydrostatic Boussinesq equations, with a linear equation of state. The initial condition consists of an analytical plane wave solution in a vertical plane, whose extension is limited by a smooth envelope both in the  $y$ - and  $z$ -direction, of width  $\simeq 1.85$  m and  $\simeq 0.9$  m respectively, to mimick the wave generator. The horizontal and vertical wavelengths are those of the laboratory experiments. At the top of the numerical domain, the boundary condition is a free surface (being solved explicitly in the Symphonie-NH code and implicitly in the NHOES code), while a free slip boundary condition is used at the bottom. At the left boundary, the incident finite extent internal gravity wave is produced thanks to a restoring layer in which all variables (velocity components and density anomaly) are restored toward the modulated analytical plane wave solution just discussed. In order to avoid spurious reflections, a sponge layer is implemented at the right boundary in which all variables are restored toward 0.

The size of the numerical domain is close to that of the laboratory experiment, namely 2.56 m in the  $x$ - direction, up to 7.68 m in the  $y$ -direction and 0.8 m in the vertical direction. The resolution of the computations is  $\Delta x \times \Delta z = 1$  cm  $\times$  0.5 cm along the  $x$  and  $z$  directions respectively, with  $\Delta y = 1$  cm in the three-dimensional code. Two-dimensional simulations with a  $\Delta x \times \Delta z = 2$  mm  $\times$  2 mm resolution have also been carried out, showing no important differences with the coarser resolution runs. For computational cost reasons, the first and coarser resolution has been retained.

The same values of the Brunt-Väisälä frequency  $N$  and of the forcing frequency  $\omega$  as in the laboratory experiments are used. The diffusivity and viscosity are molecular and isotropic and respectively equal to  $\kappa = 1.49 \times 10^{-9}$  m<sup>2</sup>s<sup>-1</sup> and  $\nu = 10^{-6}$  m<sup>2</sup>s<sup>-1</sup> (the Prandtl number is therefore equal to 700, which is the value for salted water).

#### 4. Overall behavior of the flow

A steady regime is reached in less than 10 periods, both experiments and simulations having been run for about 30 wave periods. A snapshot of the horizontal component of the velocity field  $u$  is displayed in Figure 2 in the vertical ( $x, z$ ) plane during the steady regime, for the laboratory experiment (left frame) and the corresponding two-dimensional (middle frame) and three-dimensional (right frame) simulations. The wave propagates from left to right.

<sup>1</sup>Non Hydrostatic Ocean Model for the Earth Simulator.

An apparently complex flow pattern emerges, made of (i) the incident wave, (ii) a reflected wave and second-harmonic waves of weaker amplitude in the two-dimensional simulation (and possibly in the experiment) while these waves are hardly visible in the three-dimensional simulation and (iii) a stronger signal in the interaction area between the incident and reflected waves in the three-dimensional configurations (experiment and simulation). A basic understanding of the flow requires a harmonic analysis which is now presented.

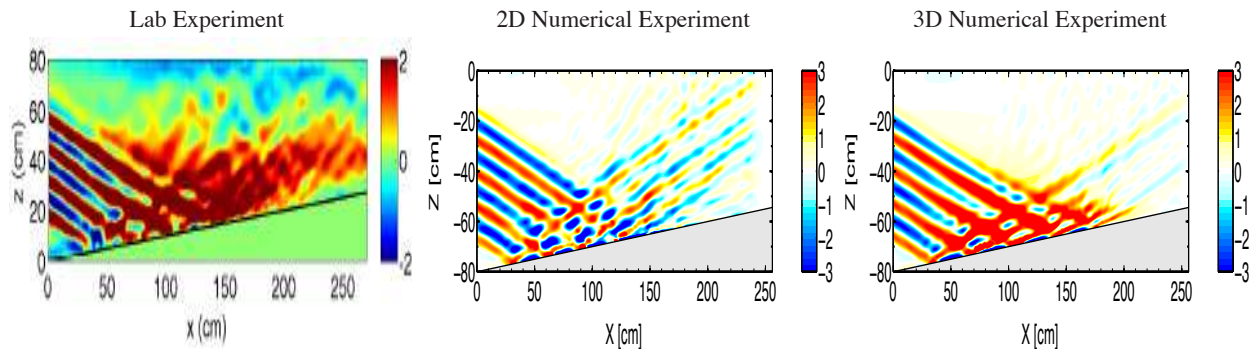


Fig. 2. Snapshot of the laboratory experiment (left) and of the corresponding two-dimensional (middle) and three-dimensional simulation (right) for the  $x$ -component of the velocity field during the steady regime, for  $N = 0.41 \text{ s}^{-1}$ ,  $\omega = 0.15 \text{ rad} \cdot \text{s}^{-1}$  and  $\alpha \approx 5.71^\circ$ . The velocity unit is  $\text{mm} \cdot \text{s}^{-1}$  and the green (left frame) and grey (middle and right frames) triangles represent the sloping boundary.

## 5. Harmonic analysis of the flow

### 5.1. First harmonic waves (incident and reflected waves)

The horizontal velocity component filtered out at the forcing frequency  $\omega$  over the last 8 periods ( $2\pi/\omega$ ) of the experiment and simulations is displayed in figure 3. This filtered field is therefore contributed by the incident and the reflected waves only. When compared with the experiment, the incident wave is remarkably reproduced by the two- and three-dimensional numerical simulations, both in structure and amplitude. An interference pattern is visible in all three frames in the area where the incident and reflected waves superimpose. Differences appear for the reflected wave: the amplitude of this wave vanishes very quickly away from the interaction area in the experiment and in the three-dimensional simulation while being present in the two-dimensional simulation, though with a weaker amplitude than the incident wave. According to linear inviscid theory, the amplitude of the reflected wave should be larger by a factor  $\gamma$  than the incident wave amplitude but its width should be smaller by the same factor, making it more sensitive to diffusive damping than the incident wave. Along with the transfer of energy toward second harmonic waves, this accounts for the observed weaker amplitude in the two-dimensional simulations [26]. It clearly appears however that a process acts in the laboratory experiment and in the three-dimensional numerical simulation which further lowers the amplitude of the reflected wave. This process should therefore be three-dimensional.

### 5.2. Second harmonic waves

The horizontal velocity component now filtered at the second harmonics of the forcing frequency ( $2\omega$ ) is plotted in Figure 4. A clear  $2\omega$ -wave has developed, whose maximum horizontal velocity is about one third of the primary wave maximum horizontal velocity. This wave results from the nonlinear interaction between the incident and reflected waves and therefore grows from the interaction area of these waves. The  $2\omega$ -wave is of larger amplitude in the two-dimensional simulation, consistent with the reflected wave being larger in this two-dimensional configuration as well, as just discussed. In the simulations, the  $2\omega$ -wave has reflected on the free surface and on the sloping boundary. We observe also that the  $2\omega$ -wave is refracted near the topography in the three-dimensional configurations and, to a lesser extent, at the free surface in the experiment, while no such refraction is visible in the two-dimensional simulation. The refraction at the free surface is due to a thin mixed layer which develops in time from the surface. As for the bottom

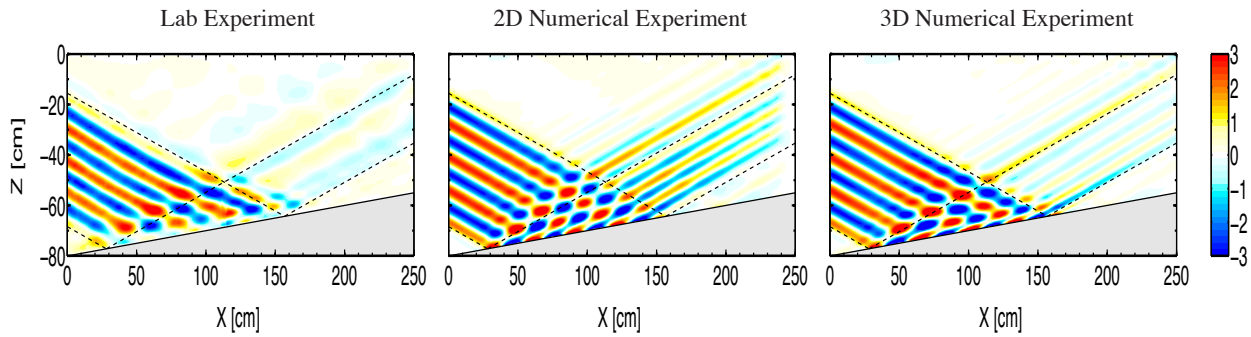


Fig. 3. Comparison of the experiment (left), two-dimensional (middle) and three-dimensional simulations (right), for the horizontal component of the velocity field filtered at the forcing frequency over the last 8 wave periods. The dotted lines mark the boundaries of the incident and reflected waves as predicted by linear inviscid theory. The experiment and simulations have been performed over 30 wave periods. The velocity unit is  $\text{mm} \cdot \text{s}^{-1}$  and the grey triangle represents the sloping boundary.

refraction, it results from the Doppler shift of the intrinsic frequency of the second harmonic wave in the interaction area, where a wave-induced mean flow grows in time, as we now discuss.

Note that no third harmonic wave component is produced since  $3\omega > N$ .

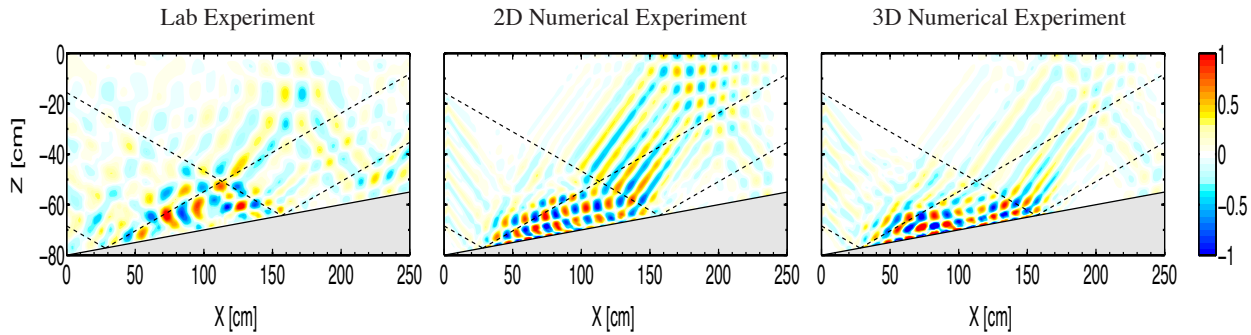


Fig. 4. Same as figure 3 except that the filtering process has been performed at twice the forcing frequency.

## 6. Wave-induced mean flow

### 6.1. Description

The mean flow is computed by a temporal average over the last 8 forcing periods and displayed in Figure 5 for the experiment and the simulations. This mean flow is therefore Eulerian and we recall that its associated Lagrangian mean flow may vanish or not; in the latter case, a net mass transport occurs. Figure 5 shows that the mean flows computed in the two- and three-dimensional simulations strongly differ. In the two-dimensional simulation, the mean flow is an along-slope current which is periodic along the direction normal to the slope. This Eulerian mean flow is generated by the interaction of the incident and reflected waves and has been predicted by [15] from a weakly nonlinear and inviscid two-dimensional analysis. We verified indeed that the wave vector normal to the slope is equal to the difference in the reflected and incident wave vector components along this direction as predicted by [15]. As noted by [15] also, the associated Lagrangian mean flow is zero in an inviscid fluid to account for the material conservation of density. We note that the amplitude of this two-dimensional mean flow is at most one third of the maximum horizontal velocity of the incident wave.

In the three-dimensional configurations by contrast, a stronger mean flow appears, which grows in time, reaches an amplitude comparable to (and even larger than) that of the incident wave and has a different structure. As recalled in section 2, this mean flow fundamentally depends upon nonlinear effects and, since it is irreversible and cumulative in time, upon dissipative effects as well (the associated Lagrangian mean flow should therefore be non zero). This mean

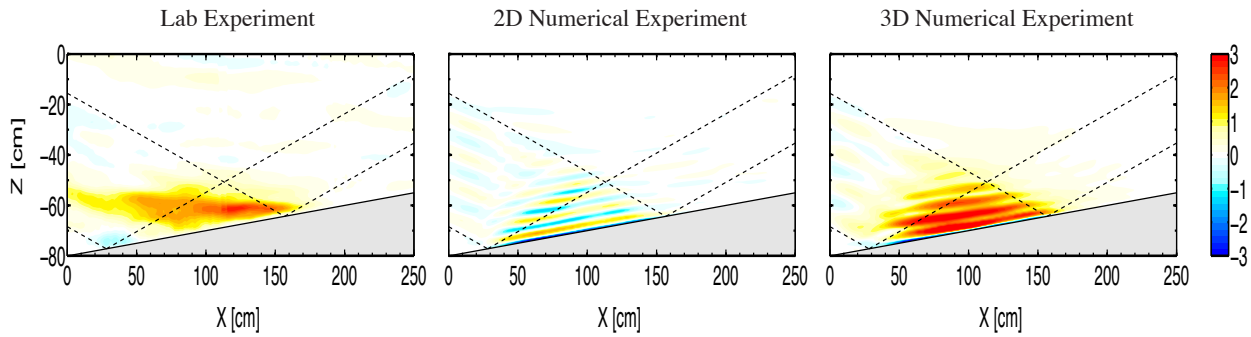


Fig. 5. Same as figure 3 except that the horizontal velocity component has been averaged over the last 8 periods of the experiment and of the numerical simulations. The Eulerian mean field is therefore displayed.

flow is horizontal, does not occur in the two-dimensional simulation but is well reproduced in the three-dimensional simulation, implying that it is intrinsically three-dimensional. Note that the signature of the two-dimensional Eulerian mean flow predicted by [15] is also visible in the three-dimensional simulation.

### 6.2. On the three-dimensional nature of the mean flow

From a theoretical point of view, the wave-induced mean flow lies along the  $x$  component of the wavevector of a two-dimensional wave propagating in a  $(x, z)$  plane ([19]). In the present case however, the medium is not homogeneous along the  $x$ -direction because of the sloping bottom. The wave generator being of finite extent along the  $y$ -direction, the wave-induced mean flow can recirculate in the horizontal plane, which gives a vertical component to the vorticity field. The distribution of potential vorticity is therefore modified. Since linear internal gravity waves do not have potential vorticity [27], the flow in the present study does not possess any potential vorticity at the initial time, when the incident wave field is generated. Because the potential vorticity is conserved by nonlinear and dissipative effects [28], the redistribution of potential vorticity by the wave dynamics should yield an even number of vortices so that the volume-averaged potential vorticity is zero [20]. In the present case the potential vorticity field is dipolar as we show now.

The potential vorticity field is displayed in figure 6 at 30 wave periods (with an average over the last period) for the three-dimensional numerical simulation, along with the associated velocity vectors. This field is organized as a dipolar structure, consisting in two vortices with a radius of the order of half the width of the envelope along the  $y$ -direction. This radius is therefore set by the length scale of problem in the  $y$ -direction, as this is expected in this non rotating case [29].

This mean flow refracts the wave field in the interaction area which leads to the distortion observed in this area in figure 4. We briefly explain below why this mean flow, along with dissipative effects (and the generation of a harmonic wave), accounts for the nearly vanishing reflected wave outside the interaction area in the experiment and in the three-dimensional simulation.

### 6.3. Theoretical approach

The equation for the acceleration of the wave-induced mean flow can be written in a two-dimensional vertical plane as a first step. In the inviscid case, this acceleration term yields the Eulerian mean current predicted by [15], whose associated Lagrangian mean flow is zero.

Further theoretical analysis shows that when viscous effects are taken into account, this Eulerian acceleration term is unchanged (except for a damping coefficient due to viscosity) and another acceleration term appears, which is proportional to the viscosity. Let us denote this term by  $A_L$ . It is contributed by the incident wave, by the reflected wave and by the interaction between those waves. It can be shown that  $A_L$  fundamentally depends upon focusing effects through the factor  $\gamma$ . Indeed, the main contribution to  $A_L$  comes from a factor  $\gamma^5$  in front of the reflected wave term while, comparatively, this coefficient is 1 for the incident wave and  $\gamma$  for the interacting term. Hence, the mean

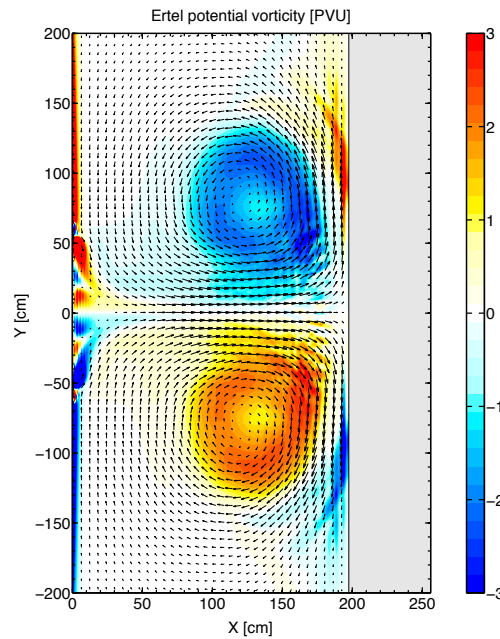


Fig. 6. Contours of the potential vorticity field at 30 wave periods (with an average over the last period) at 60 cm below the free surface.

flow present in the three-dimensional configurations is mainly fed by the reflected wave, because of focusing. Only if reflexion occurs on a flat bottom, namely  $\gamma = 1$ , does  $A_L$  become dominated by the interacting term.

## 7. Conclusion

The purpose of this work was to investigate the nonlinear reflexion of a plane wave incident onto a sloping boundary through joint laboratory experiments and numerical simulations. The simulations were first performed in a two-dimensional vertical plane and were aimed at examining the theoretical predictions of [15] about resonant interactions involving the incident, reflected and second harmonic waves [26]. The laboratory experiments performed on the Coriolis Platform soon revealed a strong discrepancy with the two-dimensional simulations because of the generation of an irreversible wave-induced mean flow in the region where the incident and reflected waves superpose. Three-dimensional simulations were then carried out, and the present work focuses on this mean flow. Preliminary results were reported in [30].

The novel result of the present work is that the acceleration of this mean flow is controlled by the focusing of the reflected wave component. As a result, the mean-flow amplitude becomes of the same order as that of the incident wave after a few wave periods or so, namely a few days in the ocean. In addition to modifying wave propagation, and to possibly leading to strongly nonlinear effects through the formation of a critical layer [31], the main property of this mean flow is mass transport, an important issue in the deep ocean where routes to fluid mixing are sought for. Note that, because mixing results in irreversible changes in the background density profile and fundamentally depends upon dissipative effects, this irreversible wave-induced mean flow may be considered as the kinematic part of mixing. Since this mean flow is created near the topography, how it would modify- or survive in- a turbulent boundary layer is certainly an important point which also deserves further study. In any case, the occurrence of such a mean flow in the ocean has been almost completely overlooked in the literature [32] and research should be launched on this issue.

## Acknowledgements

We thank Francis Auclair and H. Aiki for their help in using the Symphonie-NH code and the NHOES code they respectively developed. M. Leclair is supported by the ANR project PIWO BLAN08-1-308958. Computations have

been performed at the CINES computer center through contract c2011020580.

## References

- [1] Munk WH, Wunsch C. Abyssal recipes II: energetics of tidal and wind mixing. *Deep Sea Res.* 1998;45:1977–2010.
- [2] Alford MH, Cronin MF, M KJ. Annual cycle and depth penetration of wind-generated near-inertial internal waves at Ocean Station Papa in the Northeast Pacific. *J Phys Oceanogr.* 2012;42:889–909.
- [3] Danioux E, Klein P, P R. Propagation of wind energy into the deep ocean through a fully turbulent mesoscale eddy field. *Journal of Physical Oceanography.* 2008;38 (10):2224–2241.
- [4] Nikurashin M, Ferrari R. Radiation and dissipation of internal waves generated by geostrophic motions impinging on small-scale topography: Theory. *J Phys Oceanogr.* 2010;1055-1074:40.
- [5] Naveira Garabato AC, Polzin KL, King BA, J HK, M V. Widespread intense turbulent mixing in the Southern Ocean. *Science.* 2004;303:210–213.
- [6] Gerkema T, Staquet C, Bouruet-Aubertot P. Non-linear effects in internal-tide beams, and mixing. *Ocean Model.* 2006;12:302–318.
- [7] Bretherton FP. On the mean motion induced by internal gravity waves. *J Fluid Mech.* 1969;36:785–803.
- [8] Lighthill MJ. *Waves in Fluids.* Cambridge University Press; 1978.
- [9] Grisouard N, Buhler O. Forcing of oceanic mean flows by dissipating internal tides. *J Fluid Mech.* 2012;708:250–278.
- [10] Gortler H. Über eine schwingungserscheinung in flüssigkeiten mit stabiler dichteschichtung. *Zeitschrift für angewandte Mathematik und Mechanik.* 1943;23:65–71.
- [11] Mowbray DE, Rarity BSH. A theoretical and experimental investigation of the phase configuration of internal waves of small amplitude in a density stratified liquid. *J Fluid Mech.* 1967 Apr;28:1–16.
- [12] Phillips OM. *Dynamics of the upper ocean.* Cambridge University Press; 1966.
- [13] McPhee-Shaw EE, Kunze E. Boundary layer intrusions from a sloping bottom: a mechanism for generating intermediate nepheloid layers. *J Geophys Res.* 2002;107(C6):10.1029/2001JC000801.
- [14] Hosegood P, van Haren H. Near-bed solibores over the continental slope in the Faroe-Shetland channel. *Deep Sea Res II.* 2004;51:2943–2971.
- [15] Thorpe SA. On the reflection of a train of finite-amplitude internal waves from a uniform slope. *Journal of Fluid Mechanics.* 1987;178:279–302.
- [16] Gostiaux L, T D, Didelle H, Sommeria J, Viboud S. Quantitative laboratory observations of internal wave reflection on ascending slopes. *Physics of Fluids.* 2007;18:056602.
- [17] Rodenborn B, Kiefer D, Zhang HP, Swinney HL. Harmonic generation by reflecting internal waves. *Physics of Fluids.* 2011;23:026601.
- [18] Andrews DG, Holton JR, Leovy CB. *Middle atmosphere dynamics.* Academic Press; 1987.
- [19] Buhler O. *Waves and mean flows.* Cambridge University Press; 2009.
- [20] McIntyre ME, Norton WA. Dissipative wave-mean interactions and the transport of vorticity or potential vorticity. *J Fluid Mech.* 1990;212:403–435.

- [21] Longuet-Higgins MS. On the transport of mass by time-varying ocean currents. *Deep Sea Res.* 1969;16(5):431 – 447.
- [22] Grisouard N. Réflexions et réfractions non linéaires d'ondes internes de gravité. PhD thesis (in French), University of Grenoble, France; 2010.
- [23] Gostiaux L, Didelle H, Mercier S, Dauxois T. A novel internal waves generator. *Experiments in Fluids.* 2007;42:123–130. 10.1007/s00348-006-0225-7.
- [24] Francis A, Estournel C, Floor JW, Herrmann M, Nguyen C, Marsaleix P. A non-hydrostatic algorithm for free-surface ocean modelling. *Ocean Modelling.* 2011;36(1-2):49 – 70.
- [25] Haiki H, T Y. A numerical study on the successive formation of Meddy like lenses. *J Geophys Res.* 2004;109:C06020.
- [26] Leclair M, Staquet C. Harmonic generation by a finite-width internal gravity wave reflecting from a uniform slope. *J Fluid Mech* (submitted). 2012;.
- [27] Muller P, Holloway G, Henyey F, N P. Nonlinear interactions among internal gravity waves. *Rev Geophys.* 1986;24:493–536.
- [28] Haynes P, McIntyre ME. On the evolution of vorticity and potential vorticity in the presence of diabatic heating and frictional or other forces. *J Fluid Mech.* 1987;44:828–841.
- [29] Bordes G, Venaille A, Joubaud S, Odier P, Dauxois T. Experimental observation of a strong mean flow induced by internal gravity waves. *Physics Fluids.* 2012;In press.
- [30] Leclair M, Grisouard N, Gostiaux L, Staquet C, Auclair F. Reflexion of a plane wave onto a slope and wave-induced mean flow. In: *Proceedings of the VII International Symposium on stratified flows, Rome 22-26 August.* Editor Sapienza Università di Roma, ISBN: 9788895814490; 2011. .
- [31] Koop CG, McGee B. Measurements of internal gravity waves in a continuously stratified shear flow. *J Fluid Mech.* 1986;172:453–480.
- [32] Pinkel R, Rainville L, Klymak J. Semidiurnal Baroclinic Wave Momentum Fluxes at Kaena Ridge, Hawaii. *J Phys Oceanogr.* 2012;42(8):1249–1269.